NASA TECHNICAL NOTE

NASA TN D-3635

NASA TN D-3635

FLOW AND PRESSURE FIELD ANALYSIS OF PARALLEL GROOVE GEOMETRY FOR AN INCOMPRESSIBLE FLUID WITH CONVECTIVE INERTIA EFFECTS

by John Zuk, Lawrence P. Ludwig, and Robert L. Johnson

Lewis Research Center
Cleveland, Ohio

NATIONAL AERONAUTICS AND SPACE ADMINISTRATION • WASHINGTON, D. C. • SEPTEMBER 1966

FLOW AND PRESSURE FIELD ANALYSIS OF PARALLEL GROOVE GEOMETRY FOR AN INCOMPRESSIBLE FLUID WITH CONVECTIVE INERTIA EFFECTS

By John Zuk, Lawrence P. Ludwig, and Robert L. Johnson

Lewis Research Center
Cleveland, Ohio

NATIONAL AERONAUTICS AND SPACE ADMINISTRATION

For sale by the Clearinghouse for Federal Scientific and Technical Information
Springfield, Virginia 22151 – Price $2.00

FLOW AND PRESSURE FIELD ANALYSIS OF PARALLEL GROOVE GEOMETRY FOR AN INCOMPRESSIBLE FLUID WITH CONVECTIVE INERTIA EFFECTS

by John Zuk, Lawrence P. Ludwig, and Robert L. Johnson

Lewis Research Center

SUMMARY

A set of two-dimensional equations that includes both convective inertia and viscous forces were formulated for parallel groove geometries. The equations are solvable for the velocity and pressure distribution and optimum geometry by using numerical methods on a high-speed digital computer.

The mathematical model consisted of a smooth flat plate moving relative to a fixed parallel groove-ridge surface; both the smooth plate and the grooved plate were of infinite horizontal extent with the clearance filled with an incompressible, viscous, homogeneous, isothermal, Newtonian fluid. A modified Reynolds number evolved that is based on a groove-ridge characteristic length parallel to the smooth plate velocity vector. The analysis revealed that convective inertia can only be neglected if the modified Reynolds number is much less than 1 (creeping flow regime).

Application of the modified Reynolds number to four published experimental results reveals that a significant improvement in bearing number or sealing coefficient occurred when the modified Reynolds number was near 1. The detectable improvement in the bearing number or sealing coefficient had previously been attributed to the onset of turbulence; therefore, it is argued that the strong influence of convective inertia, and not turbulence, is the main cause of this improvement.

The consideration of convective inertia effects reveals that fluid density ρ, aspect ratio b/h_o, and number of groove-ridge pairs N are additional parameters of pressure generation dependence that are not implied in the creeping flow analysis.

The analysis presented herein provides a unified approach to parallel groove operation, which was previously covered by the creeping flow analysis and a semiempirical turbulent flow analysis. No restriction was placed on the net flow situation between the smooth and grooved plates. Therefore, the analysis and resulting equations apply equally to hydrodynamic seals, bearings, and pumps. An arbitrary groove-ridge shape is also permissible in solving the equations. Consideration of convective inertia effects explains the principle of viscoseal axial pressure generation and attainment of zero leakage.

INTRODUCTION

The parallel groove geometry has many potential applications for use as a pressure generation device. For example, the parallel groove has been applied in spiral groove thrust bearings (ref. 1), spherical and conical spiral groove bearings (ref. 1), helical groove pumps (ref. 2), and helical groove seals (viscoseal, see ref. 3).

The latter device (viscoseal) is potentially useful for sealing liquid metals, such as mercury, potassium, and sodium, in space electric power generation systems that require 1 to 3 years of unattended operation and near zero leakage (refs. 4 and 5). As pointed out in references 5 and 6, the viscoseal has inherent reliability and long life because of the absence of solid surfaces in rubbing contact.

The analysis of the spiral groove bearing in reference 1 indicates a higher load carrying capacity than the step or tilting pad bearings. An analysis of the helically grooved herringbone journal bearing is found in reference 7 for a perfect gas including the effects of small eccentricities. However, an infinite number of groove-ridge pairs was assumed for a finite-diameter journal bearing model in order to make the pressure gradients (which are discontinuous at the groove-ridge interface) a smooth varying function.

To date, analyses of parallel groove geometry have been limited to creeping flow solutions where convective inertia effects have been neglected. Convective inertia is the fluid mass acceleration due to a spatial velocity change, for example, a change in velocity due to an obstacle in the flow path. This is contrasted to an inertia effect caused by a temporal velocity change, for example, a variation in velocity at a point in a bearing due to shaft runout. The creeping flow analysis is restricted to flows where the modified Reynolds number is much less than 1; that is,

$$\mathrm{Re}^{*} = \mathrm{Re}_{L}\left(\frac{c}{L}\right)^{2} \ll 1$$

or

$$\mathrm{Re}^{*} \leq 0.01$$

where

$$\mathrm{Re}_{L} = \frac{UL}{\nu} = \frac{\rho UL}{\mu}$$

$$\frac{c}{L} < 1$$

Creeping flow analyses for pumps, screw extruders, seals, and thrust and journal bearings have been published by many authors (e.g., refs. 1 to 26). In appendix B is given an outline and discussion of the published creeping flow solutions. The main criticism of the creeping flow solution (generally used in the laminar flow regime) is that its validity is restricted to Reynolds numbers below most engineering applications and that zero net flow (seals) enters the analysis as an a priori assumption.

A number of semiempirical formulations have been devised (refs. 4, 18, 27, and 28) for the operational region beyond the creeping flow regime (turbulent regime), but they provide no insight on the effect of various parameters and give no formal approach to optimization of the geometry. The main criticism of these semiempirical analyses is that the existance of the turbulent regime is assumed; in short, turbulence is not necessary to explain reported experimental results and may not even exist. Even if turbulence does exist, convective inertia effects are thought to be far more significant. Kettleborough (ref. 29) numerically analyzed the slider bearing with inertia, turbulent, and viscous terms considered. When inertia only was considered, the results were in qualitative agreement with published (turbulent-attributed) slider bearing experimental results. Kettleborough concluded that the turbulence term did not greatly affect the operation of the slider bearing.

Golubiev (ref. 24) applied centrifugal pump similarity laws to the helical groove seal. This case considers an inviscid fluid whereby the pressure generation is found from Bernoulli's equation where ΔP varies as the square of the velocity. Due to the flow being in a confined space, and since the viscous force contributes to maintaining the generated pressure gradient, the viscous force cannot be neglected.

Unfortunately, the creeping flow optimum geometry has been extended, almost universally, to be valid for operation beyond the creeping flow regime. Since the convective inertia force is the main driving force, a complete reevaluation of the optimum geometry including the groove-ridge shape must be investigated before conclusions on viscoseal performance can be made.

The objective of this report is to examine the flow field and pressure generation in parallel groove geometries by including convective inertia effects. Since the groove steps cause convective acceleration effects of the fluid, the edges of the grooves are not neglected. A flat-plate model of infinite horizontal extent will be analyzed. This is a reasonable physical approximation because the film thicknesses (clearance gap between two relatively moving surfaces) are usually very small in comparison to the radius of curvature and the circumferential length of the pump, bearing, and seal rotors (screw extruders may be an exception to this). The significant terms for the study are found by a formal ordering procedure and by examining the physics of the problem. End effects are neglected because this is an infinite flat-plate case. (Refer to refs. 1 and 30 for creeping flow end effects and ref. 6 for experimental investigation of end effects.)

No restriction is applied as to net flow within the parallel groove geometry; therefore, the analysis applies to hydrodynamic seals, bearings, and pumps.

SYMBOLS

a	ridge or land width
b	groove width
C_p	specific heat of fluid at constant pressure
c	clearance between ridge and smooth flat plate, or radial clearance
F_x	body force in x-direction
F_y	body force in y-direction
F_z	body force in z-direction
G	dimensionless factor, function of helical geometry
h_o	step or edge height
k	thermal conductivity of fluid
L	characteristic length, length of groove-ridge pair in smooth plate relative velocity vector direction
L'	axial length, normal to plate velocity
N	number of helix starts
n	integer
ΔP	pressure differential
P^*	static pressure at reference state
P_c	static cavity pressure
Pr	Prandtl number
Q	net volume flow rate
Q_ξ	volume flow rate in plate relative velocity direction
Q_η	volume flow rate normal to plate relative velocity direction
R	radius of rotor
Re	Reynolds number
Re^*	modified or reduced Reynolds number

T^*	temperature at reference state
t	time
U	smooth flat-plate velocity
u	velocity in x-direction
V	characteristic velocity in the y-direction
$\vec{V}$	fluid velocity vector
$V_{p,x}$	pressure flow velocity in x-direction
$V_{p,z}$	pressure flow velocity in z-direction
v	velocity in y-direction
w	velocity in z-direction
x	coordinate along ridge-groove
y	coordinate across film (between plates)
z	coordinate across ridge-groove
α	angle between relative velocity direction and parallel groove-ridges or helix angle
ζ	film height
η	coordinate normal to plate relative velocity vector
Λ	bearing number
λG	empirical sealing parameter (defined in ref. 5)
μ	absolute viscosity of fluid
ν	kinematic viscosity of fluid
ν^*	kinematic viscosity of fluid at reference state
ξ	coordinate in direction of plate relative velocity vector
ρ	density
ρ^*	density at reference state
σ	shape parameter
∇	vector differential operator Del or Nabla
∇^2	Laplacian operator

Subscripts:

c	based on clearance or film thickness

g groove

L based on characteristic length

r ridge or land

ϵ plate relative velocity direction

η normal to plate velocity direction (axial length)

BASIC MODEL

The rectilinear Cartesian coordinate system was selected for mathematical tractability. A parallel groove-ridge plate geometry with a smooth flat plate moving relative to the parallel groove-ridge plate, both of infinite horizontal extent, was chosen as the basic model (see fig. 1).

Conceptually this model can be thought of as an infinitely long smooth rotor with a very large diameter and a concentric grooved housing. Actually this infinite grooved plate model is the limiting case of a helical grooved cylinder where $R \to \infty$ or $c \to 0$. If $c/R \leq 0.01$, this model should give a good qualitative picture of the flow field and pressure generation and significant trends for optimum geometry. For example, a practical

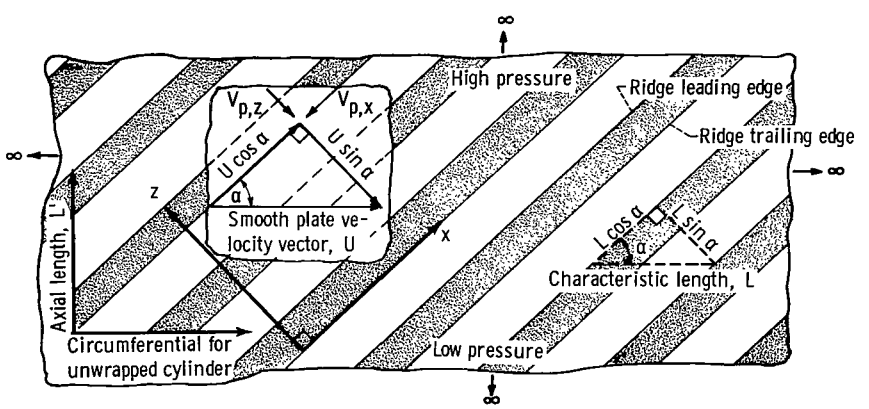

(a) Plan view.

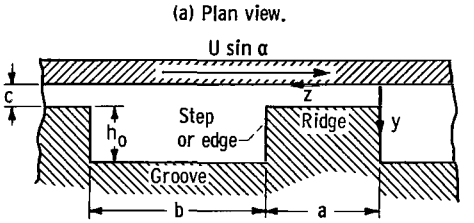

(b) Cross-sectional view along z-axis illustrating relative motion of smooth flat plate with respect to fixed parallel groove-ridge plate.

Figure 1. - Mathematical model of parallel groove-ridge geometry of infinite horizontal extent.

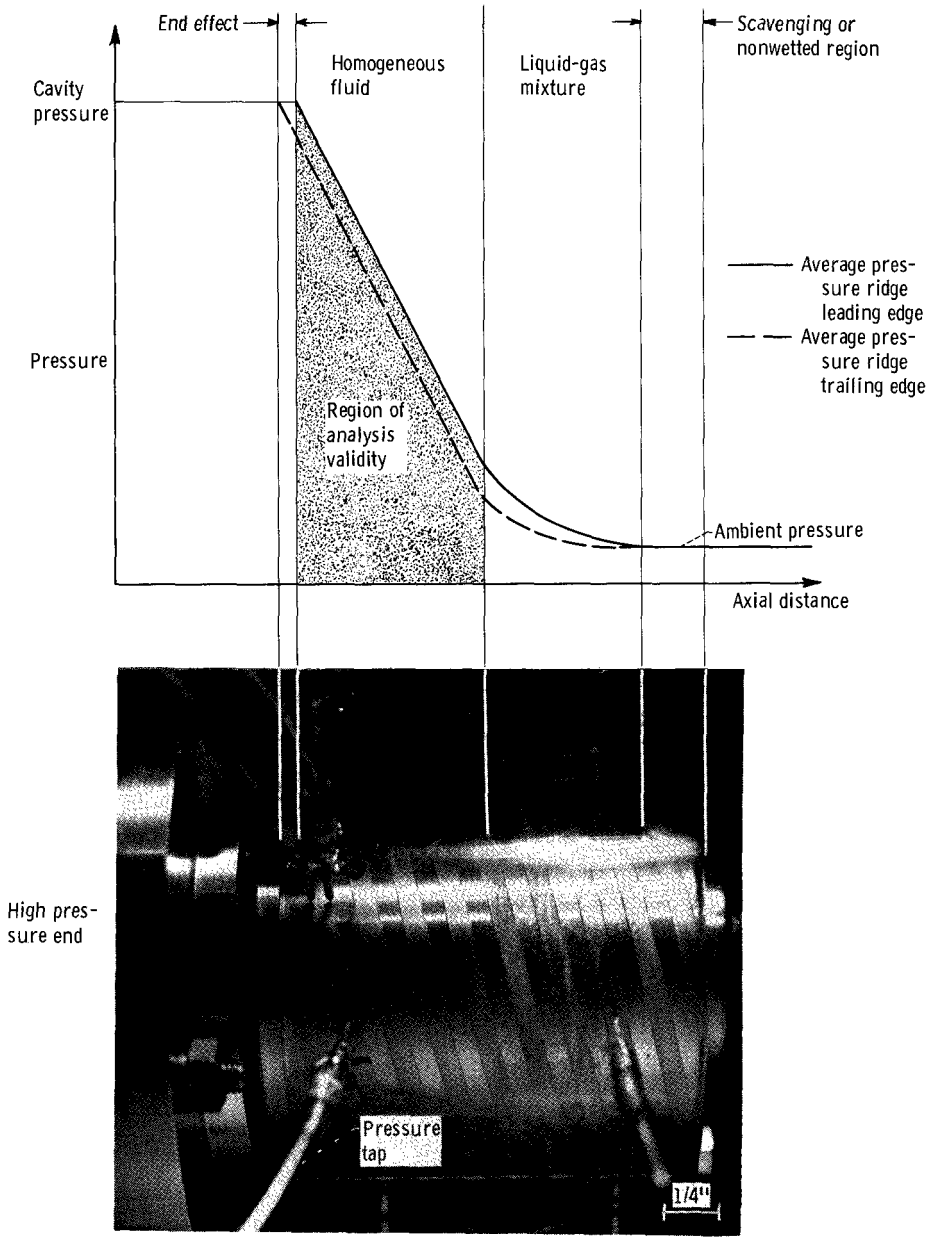

C-66-2693

Figure 2. - Region of analysis validity (homogeneous fluid) of a grooved housing viscoseal. Reynolds-number based on clearance or film thickness, 1700; modified or reduced Reynolds number, 19; 400-microinch shaft rotational movement during photographic exposure; shaft speed, 8000 rpm; sealed fluid, water.

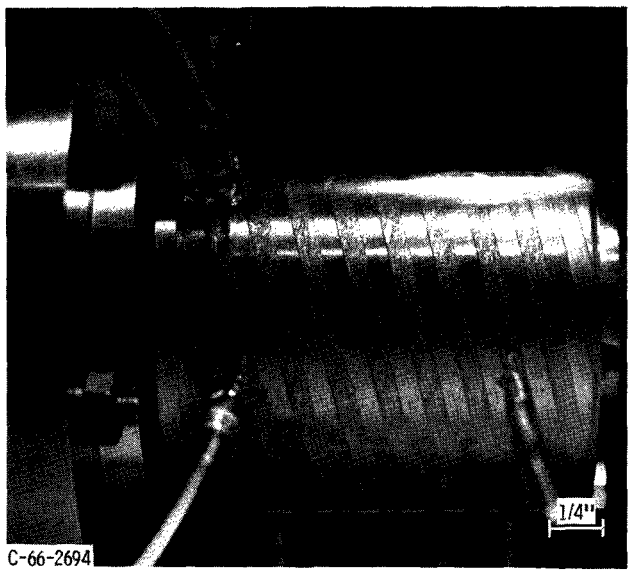

Figure 3. - Viscoseal with grooved housing operating in a regime of water-air mixture (gas ingestion). Analyses does not apply for this discontinuous fluid film case; 250-microinch shaft rotational movement during photographic exposure; shaft speed, 5000 rpm; sealed fluid, water.

geometry is a 2-inch-diameter rotor with a 0.005-inch concentric clearance, $c/R = 0.005$.

The clearance between the infinite plates is filled with any incompressible fluid, and it should be noted that for this infinite horizontal extent case there are no end effects (in practical engineering design, of course, end effects must be accounted for). Since experiments at Lewis show that the end effect zone decreases with increasing rotor speed and also that it is less than a groove width, this analysis should be valid in the bulk of the homogeneous fluid (see figs. 2 and 3).

In the flat-plate case, the boundary conditions on a groove-ridge plate in motion are constant; however, it will be advantageous to have the smooth flat plate move relative to the grooved flat plate. This will eliminate the temporal inertia terms and reduce the subsequent independent variables by one.

A word of caution for extension of the results to a case where the groove-ridge pairs on a finite shaft are rotating relative to a fixed smooth housing. The boundary conditions are different when the smooth housing is stationary and the grooved rotor is moving, and when the housing is grooved and the rotating shaft is smooth. When the rotor is grooved, the surface speed is different at each point along the step or edge of the moving boundary. Thus this analysis should be more valid for a smooth rotor and grooved fixed housing (from ref. 5 the grooved housing appears to be the desired mode of operation) with a

large radius of curvature and/or small clearance.

When referring to figure 1, it is noted that by the choice of coordinate system the groove-ridge pairs appear only in the y, z-plane. Later it will be shown that this choice of coordinate system will be necessary to reduce the analysis to a two-dimensional problem for the flow field. It should also be noted that the drag force has been resolved into its components in this coordinate system and there is no equilibrium of forces in the z-direction with inertia (nonlinear) effects neglected.

BASIC EQUATIONS

The Navier-Stokes equations for a homogeneous, incompressible, laminar, Newtonian fluid are the following (see ref. 31):

x-Direction:

$$\rho \frac{Du}{Dt} = F_x - \frac{\partial P}{\partial x} + \mu \left(\frac{\partial^2 u}{\partial x^2} + \frac{\partial^2 u}{\partial y^2} + \frac{\partial^2 u}{\partial z^2} \right) \tag{1}$$

y-Direction:

$$\rho \frac{Dv}{Dt} = F_y - \frac{\partial P}{\partial y} + \mu \left(\frac{\partial^2 v}{\partial x^2} + \frac{\partial^2 v}{\partial y^2} + \frac{\partial^2 v}{\partial z^2} \right) \tag{2}$$

z-Direction:

$$\rho \frac{Dw}{Dt} = F_z - \frac{\partial P}{\partial z} + \mu \left(\frac{\partial^2 w}{\partial x^2} + \frac{\partial^2 w}{\partial y^2} + \frac{\partial^2 w}{\partial z^2} \right) \tag{3}$$

The Eulerian or spatial derivative is D/Dt, which is composed of the local acceleration (temporal velocity change) and the convective acceleration (spatial velocity change):

$$\frac{D}{Dt} = \underbrace{\frac{\partial}{\partial t}}_{\substack{\text{Local, unsteady, or} \\ \text{nonstationary accel-} \\ \text{eration}}} + \underbrace{u \frac{\partial}{\partial x} + v \frac{\partial}{\partial y} + w \frac{\partial}{\partial z}}_{\substack{\text{Convective} \\ \text{acceleration}}}$$

The incompressible continuity equation is

$$\frac{\partial u}{\partial x} + \frac{\partial v}{\partial y} + \frac{\partial w}{\partial z} = 0 \tag{4}$$

The assumptions for this analysis are as follows:

(1) For steady flow,

$$\frac{\partial u}{\partial t} = \frac{\partial v}{\partial t} = \frac{\partial w}{\partial t} = 0$$

(2) For no body forces,

$$F_x = F_y = F_z = 0$$

This means there are no electromagnetic fields present and gravitational effects are negligible.

(3) Isothermal and equal temperature plate surface conditions are assumed.

(4) Viscous (frictional) heating is negligible. Therefore, the thermophysical properties are constant. This appears to be a good assumption for order ten (water) and smaller (liquid metals) Prandtl number Pr fluids:

$$Pr = \frac{C_p \mu}{k}$$

In experimental setups there is an inherent unsteadiness due to vibrations, shaft runout, and eccentricity of rotor with respect to housing and misalinement. These factors will influence the degree of correlation between the analytical and experimental results.

The conservation of momentum and mass equations were nondimensionalized and a formal ordering procedure was used to determine the relative magnitude of the terms. Consequently, in a formal way the negligible terms were found (see appendix A).

An important parameter, the modified or reduced Reynolds number, was found:

$$Re^* = Re_L\left(\frac{c}{L}\right)^2 = Re_c\left(\frac{c}{L}\right) \quad \text{if} \quad c/L < 1$$

This modified Reynolds number gives the relative magnitude of the inertia forces to the viscous forces; that is,

$$Re^* = \frac{\text{Inertia forces}}{\text{Viscous forces}}$$

Thus, inertia effects can be neglected only if $Re^* \leq 0.01$

After the formal ordering procedure (see appendix A), the three-dimensional flow field equations are as follows:

Conservation of momentum:

$$u\frac{\partial u}{\partial x} + v\frac{\partial u}{\partial y} + w\frac{\partial u}{\partial z} = -\frac{1}{\rho}\frac{\partial P}{\partial x} + \nu\frac{\partial^2 u}{\partial y^2} \qquad \text{(x-direction)} \tag{6}$$

$$\frac{\partial P}{\partial y} = 0 \qquad \text{(y-direction)} \tag{7}$$

$$u\frac{\partial w}{\partial x} + v\frac{\partial w}{\partial y} + w\frac{\partial w}{\partial z} = -\frac{1}{\rho}\frac{\partial P}{\partial z} + \nu\frac{\partial^2 w}{\partial y^2} \qquad \text{(z-direction)} \tag{8}$$

Conservation of mass:

$$\frac{\partial u}{\partial x} + \frac{\partial v}{\partial y} + \frac{\partial w}{\partial z} = 0 \tag{4}$$

Fully developed flow is assumed in the x-direction. This means that $\vec{V}$ and $\partial P/\partial x$ are not functions of x and that the pressure gradient in the x-direction (parallel to the groove) is a constant (verified experimentally in ref. 5). In figure 2, it is observed that this assumption is valid only where the pressure profile at the ridge leading or trailing edges in the axial direction is linear. Gas ingestion results in a nonlinear profile (see figs. 2 and 3).

With the assumption of fully developed flow along the groove-ridge direction (x-direction), the flow field equations become two-dimensional:

$$v\frac{\partial u}{\partial y} + w\frac{\partial u}{\partial z} = -\frac{1}{\rho}\frac{\partial P}{\partial x} + \nu\frac{\partial^2 u}{\partial y^2} \quad \text{where} \quad \frac{\partial P}{\partial x} = \text{constant} \tag{9}$$

$$\frac{\partial P}{\partial y} = 0 \tag{10}$$

$$v \frac{\partial w}{\partial y} + w \frac{\partial w}{\partial z} = -\frac{1}{\rho} \frac{\partial P}{\partial z} + \nu \frac{\partial^2 w}{\partial y^2} \tag{11}$$

Conservation of mass:

$$\frac{\partial v}{\partial y} + \frac{\partial w}{\partial z} = 0 \tag{12}$$

The boundary conditions for a rectangular groove are as follows:

(1)

$$\left.\begin{aligned} v &= 0 \\ u &= U \cos \alpha \\ w &= -U \sin \alpha \end{aligned}\right\} \text{ at } y = 0$$

(2)

$$u = v = w = 0 \quad \text{at} \quad c \leq y \leq c + h_o \text{ (on side of groove)}$$

$$u = v = w = 0 \quad \text{at} \quad y = c \text{ (on ridge)}$$

$$u = v = w = 0 \quad \text{at} \quad y = c + h_o \text{ (on groove root)}$$

The boundary conditions can be generalized for an arbitrary shaped groove-ridge geometry (see fig. 4):

(1)

$$\left.\begin{aligned} v &= 0 \\ u &= U \cos \alpha \\ w &= -U \sin \alpha \end{aligned}\right\} \text{ at } y = 0$$

(2)

$$u = v = w = 0 \quad \text{at} \quad y = h(z)$$

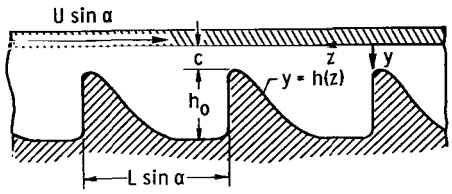

Figure 4. - Cross-sectional view along z-axis illustrating arbitrary groove-ridge pair shape.

Equations (9) to (12) can be reduced in terms of the dependent variables u, v, and w by vanishing the pressure terms. The pressure terms vanish when differentiating equations (9) and (11) with respect to y and when noting that $\partial P/\partial y = 0$ (eq. (10)). In the process the order of the equations is increased by one. The x-direction momentum equation becomes

$$\frac{\partial v}{\partial y}\frac{\partial u}{\partial y} + \frac{\partial w}{\partial y}\frac{\partial u}{\partial z} + w\frac{\partial^2 u}{\partial y \partial z} + v\frac{\partial^2 u}{\partial y^2} = \nu\frac{\partial^3 u}{\partial y^3} \tag{13}$$

The z-direction momentum equation becomes

$$\frac{\partial v}{\partial y}\frac{\partial w}{\partial y} + \frac{\partial w}{\partial y}\frac{\partial w}{\partial z} + w\frac{\partial^2 w}{\partial y \partial z} + v\frac{\partial^2 w}{\partial y^2} = \nu\frac{\partial^3 w}{\partial y^3} \tag{14}$$

Since the continuity equation remains the same,

$$\frac{\partial v}{\partial y} + \frac{\partial w}{\partial z} = 0 \tag{12}$$

then the z-direction momentum equation becomes

$$w\frac{\partial^2 w}{\partial y \partial z} + v\frac{\partial^2 w}{\partial y^2} = \nu\frac{\partial^3 w}{\partial y^3} \tag{15}$$

These equations (12), (13), and (15) can be solved for the velocity components. Once the velocity components have been obtained, the pressure gradients can be found from equations (9) and (11). Then the axial pressure gradient $\partial P/\partial L'$ can be found from

$$\frac{\partial P}{\partial L'} = \frac{\partial P}{\partial x}\sin\alpha + \left(\frac{\partial P}{\partial z}\right)_{r+g}\cos\alpha \tag{16}$$

where L' is the axial length (see fig. 5). Pressure distribution in the x- and z-directions is shown in figures 6 and 7. Therefore, by examining the analysis and the derived equations, the axial pressure gradient $\partial P/\partial L'$ is a function of (σ, U, ρ, ν), where σ is a

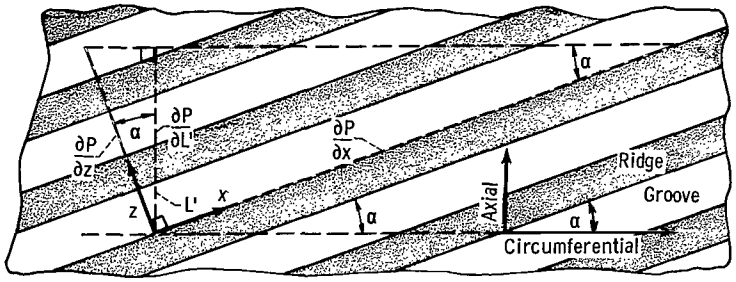

Figure 5. - Resolution of across and along groove-ridge pressure gradients into axial pressure gradient.

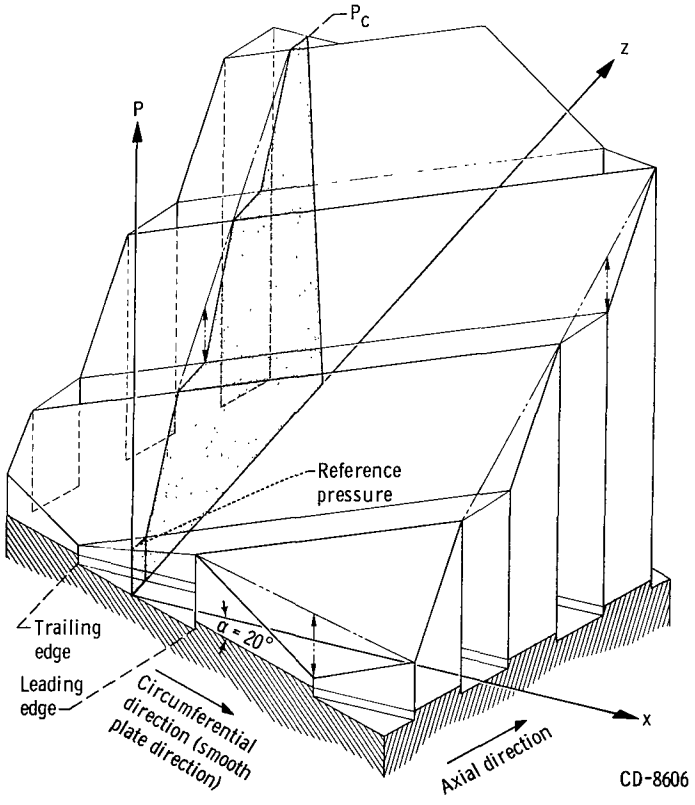

Figure 6. - Pressure distribution over parallel groove geometry. (Qualitative graphical representation from experimental data.)

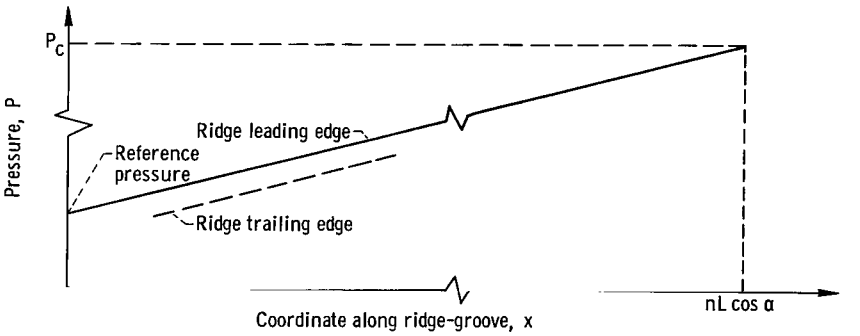

(a) Along ridges or grooves (no end effects are shown).

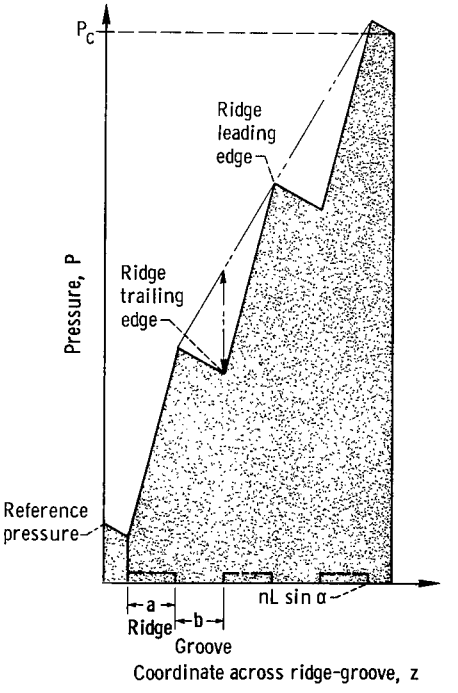

(b) Across ridges and grooves (no restriction that profile must be linear).

Figure 7. - Pressure profiles (qualitative graphical representation from experimental data).

shape parameter that is a function of (b/h_o, c/h_o, a/b, α).

Since convective inertia effects are important, new geometric parameters appear which are not implied in creeping flow theory. Most notable of these is the aspect ratio b/h_o, which implies the degree of convective effect. When the b/h_o and a/b ratios are known, N, the number of helix or groove starts, can be found. Thus the number of groove or helix starts also is an important parameter. Since inertia is important, a high density is desired for pressure generation.

DISCUSSION

Discussion of Equations

This analysis is valid only for a homogeneous fluid. Figures 2 and 3 clarify the region of validity. In some parallel groove geometries (e.g., the viscoseal) where there is a liquid-gas interface, there is a problem with gas ingestion (ref. 5). Gas ingestion, which is a condition of liquid and gas mixture throughout the seal, is shown in figure 3. The analysis is not valid for this condition because the fluid is nonhomogeneous. Further, the analysis is not valid for a scavenging area and a region consisting of a mixture of gas and liquid (see fig. 2).

It should also be pointed out that the analysis is not valid in the end effect region at the high pressure end of the seal (see fig. 2) where the groove connects with the cavity. Since the appropriate equations are nonlinear, the pressure is not a harmonic function; thus, the usual analog methods of finding end effect are not available as found in creeping flow regions (see appendix B).

The equations are unique in many ways. Mathematically, the problem has been reduced to two dimensions (y- and z-directions) but all three velocity components are present. Also, there is a pressure gradient in the third dimension (x-direction), but fortunately this gradient is a constant.

The velocity component v is no longer negligible as it was in the creeping flow solution. Physically, v cannot be negligible because of the presence of the edge effect which will result in a component of velocity in the y-direction.

Since there is no restriction on net volume flow, the pressure generation prediction equations should equally apply to hydrodynamic seals, bearings, and pumps.

When further examining the physics of the problem, it is seen that across the groove-ridge pairs the unbalance of the convective acceleration force with the drag force results in a pressure gradient in the z-direction. Since the step or edge causes the convective acceleration, its effects are not negligible unless there is a very large aspect ratio and the mathematical model accounts for the edge effect. Along the groove and

ridge (x-direction) the drag force is in equilibrium with the induced pressure and convective inertia force. The drag force not only causes fluid motion but also aids in maintaining equilibrium with the pressure along the groove or ridge.

Both equations of motion illustrate the coupling of u, v, and w in the convective inertia terms. This means that physically a condition such as no end leakage is possible. In creeping flow there is no coupling between the velocity components, which illustrates the shortcoming of that analysis (i. e., end leakage is not zero).

The assumption that the inertia terms are of the same order as the viscous terms results in equations of the boundary layer type; however, the boundary conditions are different.

The equations are of a form that might tempt one to reduce the number of independent variables by one by trying to find the admissable flow field which would result in a similarity transform solution. This technique fails because of the characteristic lengths that are present in this type of confined flow.

The equations are solvable by using high-speed digital computer numerical methods. A mathematical function to describe the groove-ridge shape would be too complex for a closed-form analytical solution. It should be interesting to find out if the step is still the optimum shape with convective inertia effects included. For creeping flow, Lord Rayleigh found in 1912 that the step was the optimum shape by using calculus of variations.

The equations and ordering procedure should be reexamined carefully before extending these results beyond the assumptions used in this analysis.

Discussion of Modified Reynolds Number

A check was made on the significance of the modified or reduced Reynolds number by calculating Re^* from the available published data at the claimed onset of turbulence (break point). In table I it can be noted that the departure in all cases from a constant sealing coefficient occurred when Re^* was in the range of 0. 26 to 2. 2, which suggests that the so-called beginning of turbulent operation is really the beginning of significant convective inertia effects. This would be in agreement with Kettleborough (ref. 29), who found qualitative agreement between his inertia solution and experimental turbulent results.

For seals 5, 6, and 7 (see ref. 27 and table I), only the groove to ridge ratio has changed. As the ratio increases, the breakpoint decreases. This is reasonable since a larger ridge area results in a less influential convective inertia effect and delays the beginning of pronounced convective inertia effects. It can also be seen in table I that the calculated Re^* are within an order of magnitude of one another for all of the experi-

TABLE I. - CRITICAL MODIFIED REYNOLDS NUMBER FOR ONSET OF TURBULENCE OF VARIOUS EXPERIMENTERS

Experimenter	Reference	Seal	Diameter, in.	Radial clearance, c, in.	Ratio of radial clearance to rotor radius, c/R	Ridge width, a, in.	Groove width, b, in.	Helix angle, α, deg	Characteristic length, L, in.	Clearance Reynolds number, Re_c	Modified Reynolds number, Re*
Stair	27	[a]1	1.2430	0.0042	0.0068	0.0934	0.1596	14.5	1.01	400	1.7
		2	1.2465	.00235	.0038	.1176	.0494	9.67	.98	(b)	(b)
		2B	1.2420	.0047	.0076	.1176	.0494	9.67	.98	(b)	(b)
		3	1.2461	.00265	.0043	.0828	.0842	9.67	.98	350	.95
		3B	1.2408	.0053	.0085	.0828	.0842	9.67	.98	(b)	(b)
		4	1.2461	.00265	.0043	.0514	.1156	9.67	.98	200	.95
		4B	1.2408	.0053	.0085	.0514	.1156	9.67	.98	400	2.2
		5	1.2455	.00295	.0047	.1585	.0607	5.81	1.83	600	.97
		6	1.2455	.00295	.0047	.1070	.1083	5.81	1.83	200	.32
		7	1.2455	.00295	.0047	.0609	.1600	5.81	1.83	160	.26
King	4 and 27	3C	2	0.0029	0.0029	0.1063	0.1063	3.86	3.2	550	0.50
		1B	2	.0020	.0020	.1063	.1063	3.86	3.2	400	.25
		2E	2	.0025	.0020	.1000	.1000	7.26	1.54	650	1.1
		5D	2	.0015	.0015	.1000	.1000	7.26	1.54	650	.63
McGrew and McHugh	18	SF96-5 oil	1	0.00325	0.0065	(c)	(c)	14.5	3.14	400	0.41
Lessley	28	Configuration B	2	0.0032	0.0032	0.075	0.122	14.5	0.79	350	1.4
		Configuration C	2	.0032	.0032	.083	.136	4	3.13	500	.51

[a]Eccentricity of rotor to housing, $\epsilon = 0.1$.

[b]Break point not well defined.

[c]Four thread starts.

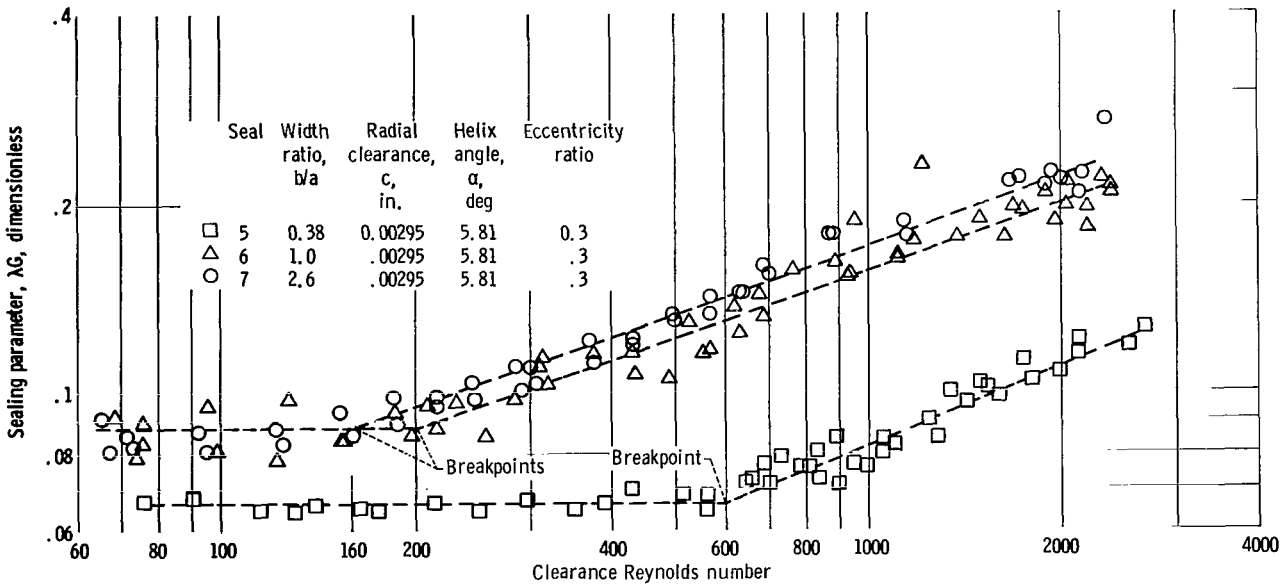

Figure 8. - Experimental sealing parameter for seals 5, 6, and 7 from reference 27.

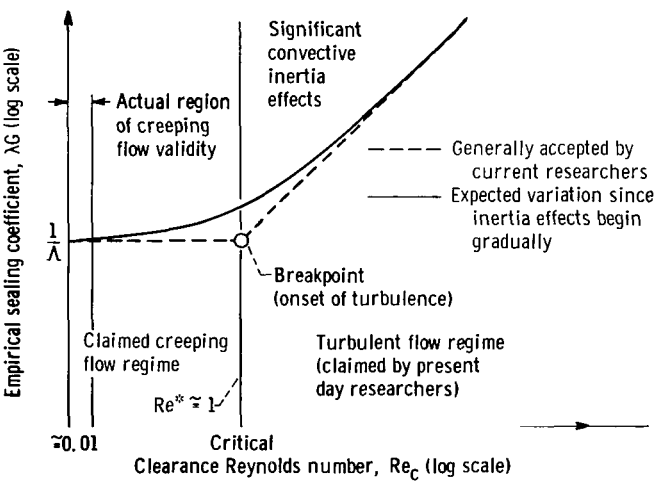

Figure 9. - Empirical sealing coefficient as function of clearance Reynolds number.

menters. It is difficult, nevertheless, to select the breakpoint (see fig. 8). Even in a range of possible breakpoint numbers, however, the order of magnitude will remain the same. Further experimental results will be necessary, but in general, it can be concluded that if $Re^* \geq 1$, a constant sealing coefficient or bearing number will not exist.

In figure 9 it is seen that classically the empirical sealing parameter λG was thought to be a constant until some critical Re_c and then to vary exponentially in the turbulent regime. The creeping flow solution was thought to be valid until the critical Re_c and then a semiempirical turbulent theory had to be used. Actually, the onset of significant convective inertia should be gradual, as shown in figure 9. Data (from ref. 27) for seal 7 in figure 8 tends to show this. The derived equations herein pertain to all cases under the assumptions stated

and will break down only under strong turbulence or an unknown instability pnenomena.

Principle of Viscoseal Operation

The classical explanation of viscoseal operation is now described. Since the seal is "pumping" the sealed fluid as fast as it is leaking out, there is no net end flow (zero leakage). From the basic laws of fluid mechanics, however, it is seen that the viscoseal axial pressure gradient results from the unbalance of the convective inertia force across the groove-ridge pairs and the drag force. The convective inertia force is much greater than the opposing drag force and results in a net pressure force. Along the groove-ridge direction, the drag force maintains equilibrium with the pressure force and convective inertia force. All three velocity components are "coupled", and thus zero net leakage is achieved. This is an excellent example of the physical importance of a nonlinear effect. The inadequacy of the linear theory (creeping flow) has been previously discussed.

CONCLUDING REMARKS

A review of the literature on analysis of the parallel groove geometry revealed that either the convective inertia forces or the viscous forces were neglected (inviscid fluid assumption). This analysis included both convective inertia and viscous forces. The following two-dimensional set of flow field equations were formulated and are solvable for the velocity and pressure distribution and optimum geometry utilizing numerical methods on a high-speed digital computer:

Conservation of momentum:

$$v\frac{\partial u}{\partial y} + w\frac{\partial u}{\partial z} = -\frac{1}{\rho}\frac{\partial P}{\partial x} + \nu\frac{\partial^2 u}{\partial y^2} \qquad \frac{\partial P}{\partial x} = \text{constant} \tag{9}$$

$$\frac{\partial P}{\partial y} = 0 \tag{10}$$

$$v\frac{\partial w}{\partial y} + w\frac{\partial w}{\partial z} = -\frac{1}{\rho}\frac{\partial P}{\partial z} + \nu\frac{\partial^2 w}{\partial y^2} \tag{11}$$

Conservation of mass:

$$\frac{\partial v}{\partial y} + \frac{\partial w}{\partial z} = 0 \tag{12}$$

With boundary conditions at the moving smooth plate surface,

$$u = U \cos \alpha$$

$$v = 0$$

$$w = -U \sin \alpha$$

With boundary conditions at the fixed parallel groove geometry surface,

$$u = v = w = 0$$

From the development and analysis of the equations, the following results and conclusions can be made:

1. A modified or reduced Reynolds number evolved which gives the relative magnitude of the convective inertia forces to the viscous forces:

$$Re^* \equiv Re_L \left(\frac{c}{L}\right)^2 \equiv Re_c \left(\frac{c}{L}\right) \quad \text{if} \quad \frac{c}{L} < 1$$

The characteristic length was selected to be the length of the groove-ridge pair in the direction of the smooth plate velocity vector. This is the principle length over which the driving force acts. The flow behavior over each groove-ridge pair is the same. Convective inertia effects can only be neglected if $Re^* \ll 1$, which will result in true creeping flow.

2. A modified Reynolds number equal to 1 will predict a significant change in sealing coefficient or bearing number which heretofore was attributed to the onset of turbulence. This means that the convective inertia effects are the foremost contributing factor to the improvement in sealing coefficient or bearing number, not the turbulence effects. A calculation of the modified Reynolds number at the onset of turbulence of four different experimenters disclosed that the modified Reynolds number was near 1 ($Re^* = 0.25$ to2.2).

3. Several additional parameters of pressure generation dependence where found that are not implied in the creeping flow analysis. These additional parameters, which

arise from convective inertia effects, are the fluid density ρ, the groove width to depth or aspect ratio b/h_0, and the number of groove-ridge pairs N.

4. Solving equations (9) to (12) by numerical analysis will permit the investigation of arbitrary groove-ridge shape, for example, sinusoidal, rectangular, triangular, etc. (It is expected that the optimum groove-ridge geometry will be different from that found from the creeping flow solution.) Now a check can be made to see if a step is the optimum shape with convective inertia effects as it is for creeping flow.

5. The analysis provides a unified approach to parallel groove operation previously covered by creeping flow (sometimes called laminar flow) analysis and a semiempirical turbulent flow analysis.

6. No restriction was placed on the net flow situation between the plates. Therefore, the analysis can be used to analyze parallel groove geometries in hydrodynamic seals, bearings, and pumps.

7. The viscoseal axial pressure gradient results from the unbalance of the convective inertia force across the groove-ridge pairs and the drag force. Along the grooves or ridges, the drag force maintains equilibrium with the pressure force and the convective inertia force.

8. Zero leakage in viscoseal analysis can be attained through the consideration of convective acceleration terms (nonlinear effect). It is argued that the creeping flow analysis, which is a linear theory, cannot prove zero leakage.

9. The format of this analysis can be used to evaluate qualitative convective inertia effects in any step or converging wall hydrodynamic seal, pump, or bearing (Rayleigh step, journal bearing, etc.).

Lewis Research Center,
National Aeronautics and Space Administration,
Cleveland, Ohio, June 26, 1966,
120-27-04-03-22.

APPENDIX A

FORMAL ORDERING PROCEDURE FOR SIMPLIFYING BASIC EQUATIONS

The Navier-Stokes equations for a homogeneous incompressible Newtonian fluid, neglecting body forces and for steady flow, are

$$\rho\left(u\frac{\partial u}{\partial x}+v\frac{\partial u}{\partial y}+w\frac{\partial u}{\partial z}\right)=-\frac{\partial P}{\partial x}+\mu\left(\frac{\partial^2 u}{\partial x^2}+\frac{\partial^2 u}{\partial y^2}+\frac{\partial^2 u}{\partial z^2}\right) \tag{A1}$$

$$\rho\left(u\frac{\partial v}{\partial x}+v\frac{\partial v}{\partial y}+w\frac{\partial v}{\partial z}\right)=-\frac{\partial P}{\partial y}+\mu\left(\frac{\partial^2 v}{\partial x^2}+\frac{\partial^2 v}{\partial y^2}+\frac{\partial^2 v}{\partial z^2}\right) \tag{A2}$$

$$\rho\left(u\frac{\partial w}{\partial x}+v\frac{\partial w}{\partial y}+w\frac{\partial w}{\partial z}\right)=-\frac{\partial P}{\partial z}+\mu\left(\frac{\partial^2 w}{\partial x^2}+\frac{\partial^2 w}{\partial y^2}+\frac{\partial^2 w}{\partial z^2}\right) \tag{A3}$$

The incompressible continuity equation is

$$\frac{\partial u}{\partial x}+\frac{\partial v}{\partial y}+\frac{\partial w}{\partial z}=0 \tag{A4}$$

To find the important terms in the previous flow field equations, a formal ordering procedure will be used to determine the relative magnitudes of the terms.

The terms are normalized by scaling them to their appropriate maximum characteristic value as follows: let

$$\bar{x}=\frac{x}{L\cos\alpha} \qquad \bar{y}=\frac{y}{c} \qquad \bar{z}=\frac{z}{L\sin\alpha}$$

$$\bar{u}=\frac{u}{U\cos\alpha} \qquad \bar{v}=\frac{v}{V} \qquad \bar{w}=\frac{w}{U\sin\alpha}$$

The characteristic dimensions can be seen in figure 1. It is noted that a trigonometric relation exists between the x and z characteristic lengths and that $c/L < 1$. The characteristic length was selected to be the length of the groove-ridge pair in the direction of the smooth plate velocity vector. This is the principle length over which

the driving force acts. The flow behavior over each groove-ridge pair is the same.

Let ρ^* and ν^* be the fluid density and viscosity corresponding to a reference state (P^*, T^*). Therefore,

$$\overline{\nu} = \frac{\nu}{\nu^*} = 1$$

and

$$\overline{\rho} = \frac{\rho}{\rho^*} = 1$$

for incompressible fluids with constant thermophysical properties. Now to find the relative magnitude of V so that all terms of the incompressible continuity equation will be of the same order, the incompressible continuity equation is nondimensionalized:

$$\frac{\partial \overline{u}}{\partial \overline{x}} + \frac{V}{U}\frac{L}{c}\frac{\partial \overline{v}}{\partial \overline{y}} + \frac{\partial \overline{w}}{\partial \overline{z}} = 0 \qquad \text{(A5)}$$

To have all terms of the equation the same order of magnitude, $\frac{V}{U}\frac{L}{c}$ must be of the order of 1. Therefore, $V = U\frac{c}{L}$, and thus $\overline{v} = \frac{v}{U}\frac{L}{c}$.

Next the equations of motion are nondimensionalized. The pressure term must first be nondimensionalized; even though the pressure is not the driving force, it is the function of primary importance. Thus the characteristic pressure is not extremely important. Since the pressure gradient is related to the rotor speed, it appears to be logical to nondimensionalize the pressure with respect to the dynamic pressure ρU^2 (also called the dynamic head):

$$\overline{P} = \frac{P}{\rho U^2}$$

It can be seen that the characteristic dynamic pressure ρU^2 has reduced the number of nondimensional groups by one (i.e., if P^* (a reference pressure) had been used, another nondimensional group would be present in the equations). Also, since the incompressible case is being analyzed, the pressure appears in the dynamic role only, not in the thermodynamic role.

When the x-direction momentum equation is nondimensionalized, equation (1) results in

$$\bar{u}\frac{\partial\bar{u}}{\partial\bar{x}}+\bar{v}\frac{\partial\bar{u}}{\partial\bar{y}}+\bar{w}\frac{\partial\bar{u}}{\partial\bar{z}}=-\frac{1}{\cos^2\alpha}\frac{\partial\bar{P}}{\partial\bar{x}}+\frac{\nu^*}{UL}\left[\frac{1}{\cos^2\alpha}\frac{\partial^2\bar{u}}{\partial\bar{x}^2}+\left(\frac{L}{c}\right)^2\frac{\partial^2\bar{u}}{\partial\bar{y}^2}+\frac{1}{\sin^2\alpha}\frac{\partial^2\bar{u}}{\partial\bar{z}^2}\right]$$

Next a Reynolds number is defined based on the characteristic length L:

$$\mathrm{Re}_L=\frac{UL}{\nu^*}$$

where

$$\nu=\nu^*\bar{\nu}=\nu^*$$

and thus

$$\bar{u}\frac{\partial\bar{u}}{\partial\bar{x}}+\bar{v}\frac{\partial\bar{u}}{\partial\bar{y}}+\bar{w}\frac{\partial\bar{u}}{\partial\bar{z}}=-\frac{1}{\cos^2\alpha}\frac{\partial\bar{P}}{\partial\bar{x}}+\frac{1}{\mathrm{Re}_L}\left[\frac{1}{\cos^2\alpha}\frac{\partial^2\bar{u}}{\partial\bar{x}^2}+\left(\frac{L}{c}\right)^2\frac{\partial^2\bar{u}}{\partial\bar{y}^2}+\frac{1}{\sin^2\alpha}\frac{\partial^2\bar{u}}{\partial\bar{z}^2}\right]$$

The convective acceleration and pressure terms are of unit order; thus, the viscous term must be of unit order also. The largest term of the viscous forces is $\left(\frac{L}{c}\right)^2\frac{\partial^2\bar{u}}{\partial\bar{y}^2}$, since $\left(\frac{c}{L}\right)<1$; therefore, the $\frac{1}{\mathrm{Re}_L}\left(\frac{L}{c}\right)^2$ should be of unit order. The modified Reynolds number is defined by $\mathrm{Re}^*\equiv\mathrm{Re}_L\left(\frac{c}{L}\right)^2$. This is the identical "reduced" or "effective" Reynolds number that is used in the bearing theory to show the true relative magnitude of the inertia and viscous forces; therefore,

$$\mathrm{Re}^*=\frac{\text{Inertia forces}}{\text{Viscous forces}}$$

(e.g., see ref. 31). Now for curved geometries, a Reynolds number based on clearance has appeared. This is especially true in viscoseal analysis where

$$\mathrm{Re}_c=\frac{Uc}{\nu}$$

Writing the previous x-direction momentum equation in terms of Re_c gives

$$\bar{u}\frac{\partial\bar{u}}{\partial\bar{x}}+\bar{v}\frac{\partial\bar{u}}{\partial\bar{y}}+\bar{w}\frac{\partial\bar{u}}{\partial\bar{z}}=-\frac{1}{\cos^2\alpha}\frac{\partial\bar{P}}{\partial\bar{x}}+\frac{\nu^*}{Uc}\left(\frac{c}{L}\frac{1}{\cos^2\alpha}\frac{\partial^2\bar{u}}{\partial\bar{x}^2}+\frac{L}{c}\frac{\partial^2\bar{u}}{\partial\bar{y}^2}+\frac{c}{L}\frac{1}{\sin^2\alpha}\frac{\partial^2\bar{u}}{\partial\bar{z}^2}\right)$$

or

$$\bar{u}\frac{\partial\bar{u}}{\partial\bar{x}}+\bar{v}\frac{\partial\bar{u}}{\partial\bar{y}}+\bar{w}\frac{\partial\bar{u}}{\partial\bar{z}}=-\frac{1}{\cos^2\alpha}\frac{\partial\bar{P}}{\partial\bar{x}}+\frac{1}{Re_c}\left(\frac{c}{L}\frac{1}{\cos^2\alpha}\frac{\partial^2\bar{u}}{\partial\bar{x}^2}+\frac{L}{c}\frac{\partial^2\bar{u}}{\partial\bar{y}^2}+\frac{c}{L}\frac{1}{\sin^2\alpha}\frac{\partial^2\bar{u}}{\partial\bar{z}^2}\right)$$

Again it is seen that the $\partial^2\bar{u}/\partial\bar{y}^2$ term is the largest.

Thus $1/Re_c(L/c)$ should be of unit order. Now

$$Re^* \equiv Re_c\left(\frac{c}{L}\right)$$

which leads to

$$Re^* \equiv Re_L\left(\frac{c}{L}\right)^2 \equiv Re_c\left(\frac{c}{L}\right)$$

It does not matter which Reynolds number is used to find the relative inertia force to viscous force ratio provided that $c/L < 1$, which corresponds to the conditions

$$\frac{\partial^2}{\partial y^2} >> \frac{\partial^2}{\partial z^2}$$

and

$$\frac{\partial^2}{\partial y^2} >> \frac{\partial^2}{\partial x^2}$$

The proper x-direction momentum equation then becomes

$$u\frac{\partial u}{\partial x}+v\frac{\partial u}{\partial y}+w\frac{\partial u}{\partial z}=-\frac{1}{\rho}\frac{\partial P}{\partial x}+\mu\frac{\partial^2 u}{\partial y^2} \tag{A6}$$

It is assumed that α does not go to 0° or 90° for the formal ordering procedure to be valid.

Example

A numerical example will be used to illustrate the validity of neglecting the $\partial^2/\partial z^2$ and $\partial^2/\partial x^2$ viscous terms. A typical viscoseal has the following construction and operating conditions: smooth 2-inch-diameter rotor, 0.0035-inch concentric radial clearance between the ridge (housing) and rotor surfaces, 1000 rpm, and sealed fluid (water) at 60° F, where

$\nu = 17.5\times10^{-4}$ sq in./sec

c = 0.0035 in.

U = 2πR(1000 rpm)/60 = 100 in./sec (plate speed)

c/R = 0.0035 (therefore, curvature effects should be slight)

L = Ridge width + Groove width (in circumferential direction)
= 0.2 in. + 0.2 in. = 0.4 in.

$\alpha = 15^\circ$

$Re_L = UL/\nu = 23\ 000$

$Re_c = Uc/\nu = 200$

Using the Reynolds number based on the characteristic length L yields

$$\frac{1}{Re_L}\left[\frac{1}{\cos^2\alpha}\frac{\partial^2\bar{u}}{\partial\bar{x}^2}+\left(\frac{L}{c}\right)^2\frac{\partial^2\bar{u}}{\partial\bar{y}^2}+\frac{1}{\sin^2\alpha}\frac{\partial^2\bar{u}}{\partial\bar{z}^2}\right]=\frac{1}{Re_L}\left(1.1\frac{\partial^2\bar{u}}{\partial\bar{x}^2}+13\ 000\frac{\partial^2\bar{u}}{\partial\bar{y}^2}+15\frac{\partial^2\bar{u}}{\partial\bar{z}^2}\right)$$

Using the Reynolds number based on the clearance c gives

$$\frac{1}{Re_c}\left[\left(\frac{c}{L}\right)\frac{1}{\cos^2\alpha}\frac{\partial^2\bar{u}}{\partial\bar{x}^2}+\left(\frac{L}{c}\right)\frac{\partial^2\bar{u}}{\partial\bar{y}^2}+\left(\frac{c}{L}\right)\frac{1}{\sin^2\alpha}\frac{\partial^2\bar{u}}{\partial\bar{z}^2}\right]=\frac{1}{Re_c}\left(0.01\frac{\partial^2\bar{u}}{\partial\bar{x}^2}+114\frac{\partial^2\bar{u}}{\partial\bar{y}^2}+0.13\frac{\partial^2\bar{u}}{\partial\bar{z}^2}\right)$$

In both equations it is seen that $\partial^2\bar{u}/\partial\bar{y}^2$ is the largest term. Now the modified or reduced Reynolds number is

$$Re^* = Re_L\left(\frac{c}{L}\right)^2 = Re_c\left(\frac{c}{L}\right) = 1.75$$

Nondimensionalization of y- and z-Direction Momentum Equations

Nondimensionalizing the y-direction momentum equation (eq. (2)) yields

$$\bar{u}\frac{\partial\bar{v}}{\partial\bar{x}}+\bar{v}\frac{\partial\bar{v}}{\partial\bar{y}}+\bar{w}\frac{\partial\bar{v}}{\partial\bar{z}}=-\left(\frac{L}{c}\right)^2\frac{\partial\bar{P}}{\partial\bar{y}}+\frac{1}{Re_L c}\left[\frac{1}{\cos^2\alpha}\frac{\partial^2\bar{v}}{\partial\bar{x}^2}+\left(\frac{L}{c}\right)^2\frac{\partial^2\bar{v}}{\partial\bar{y}^2}+\frac{1}{\sin^2\alpha}\frac{\partial^2\bar{v}}{\partial\bar{z}^2}\right]$$

Again using the definition of Re^* and comparing the largest terms give

$$\frac{1}{Re^*}\frac{\partial^2\bar{v}}{\partial\bar{y}^2}\sim 0(1)$$

and

$$\left(\frac{L}{c}\right)^2\frac{\partial\bar{P}}{\partial\bar{y}}=\frac{1}{Re_L}\left(\frac{L}{c}\right)^2\frac{\partial^2\bar{v}}{\partial\bar{y}^2}$$

Since

$$\frac{1}{Re_L}<<1$$

therefore

$$\frac{\partial P}{\partial y} \cong 0 \tag{A7}$$

This result is expected for a flat plate where there is no mechanism to generate a radial pressure gradient (e.g., a centrifugal force). For small curvatures, however, the radial pressure gradient $\partial P/\partial y$ should also be a small quantity and have little physical influence on the axial pressure gradient.

In a similar manner the z-direction momentum equation is nondimensionalized and the result is

$$u\frac{\partial w}{\partial x} + v\frac{\partial w}{\partial y} + w\frac{\partial w}{\partial z} = -\frac{1}{\rho}\frac{\partial P}{\partial z} + \mu\frac{\partial^2 w}{\partial y^2} \tag{A8}$$

As expected, due to dimensions of the same relative size, the z-direction momentum equation is the same as the x-direction momentum equation (eq. (6)), but the boundary conditions are different.

APPENDIX B

SUMMARY OF CREEPING FLOW ANALYSIS

The optimization from creeping flow analysis has been formulated by considering a flat-plate model (unwrapped cylinders, see fig. 10) and the following:

(1) General incompressible plane Couette flow is assumed in the ξ-direction (Poiseuille flow and simple Couette flow). The ξ-direction momentum equation is

$$\frac{\partial^2 u_\epsilon}{\partial \zeta^2} = \frac{1}{\mu} \frac{\partial P}{\partial \xi}$$

with the boundary conditions

$$u_\epsilon = U \quad \text{at} \quad \zeta = 0$$

$$u_\epsilon = 0 \quad \text{at} \quad \zeta = h$$

where

$$h = c \quad \text{at ridge surface}$$

$$h = c + h_o \quad \text{at groove root surface}$$

The well known solution (e.g., see ref. 31) is

$$u_\epsilon = \frac{\zeta}{h} U - \frac{h}{2\mu} \frac{dP}{d\xi} \zeta \left(1 - \frac{\zeta}{h}\right)$$

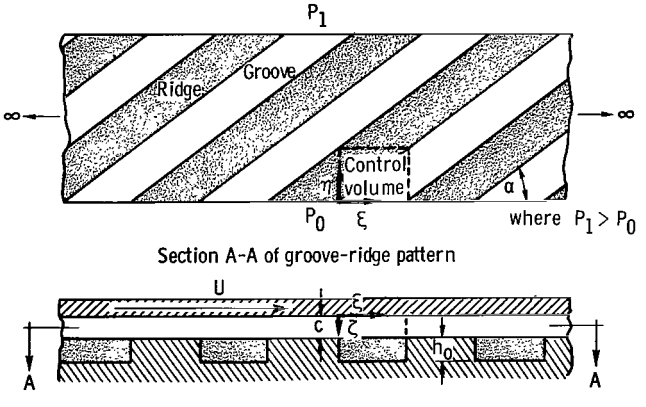

Figure 10. - Model used in creeping flow solution.

(2) Poiseuille flow is assumed in the η-direction. The η-direction momentum equation is

$$\frac{\partial^2 w_\eta}{\partial \zeta^2} = \frac{1}{\mu} \frac{\partial P}{\partial \eta}$$

with the boundary conditions

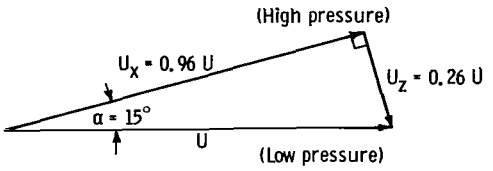

Figure 11. - Resolution of plate velocity (or drag force) into components along and across groove or ridge.

$$w_\eta = 0 \quad \text{at} \quad \zeta = 0$$

$$w_\eta = 0 \quad \text{at} \quad \zeta = h$$

The well known solution (see ref. 31) is

$$w_\eta = \frac{1}{2\mu}\left(\frac{\partial P}{\partial \eta}\right)\zeta(\zeta - h)$$

Now the condition $Q = 0$ is imposed in the control volume; that is,

$$Q = Q_\xi + Q_\eta = \iint u_\epsilon \, d\eta \, d\zeta + \iint w_\eta \, d\zeta \, d\xi = 0$$

which means that there is no net end leakage or closed channel flow. This is a restriction that limits the optimization and pressure gradient prediction to a seal only.

Solving for pressure gradient that satisfies the Reynolds equation (ref. 32) results in a sealing parameter

$$\frac{\Delta P}{L'} = \frac{6\mu UG}{c^2}$$

or

$$G = \frac{c^2}{6\mu U}\left(\frac{\Delta P}{L'}\right) = \frac{1}{\Lambda}$$

where Λ is the bearing number (ref. 32) and G is a geometry factor. See references 1 to 26 for various expressions and values for G.

The creeping flow analysis has some paradoxes. It can best be illustrated by referring to figures 1 and 11 and by observing the resolution of the drag force into components along the groove (x-direction) and normal to the groove (z-direction). In creeping flow, the drag force is in equilibrium with the pressure force. Thus along the groove (x-direction) the drag force is indeed in equilibrium with the pressure force. In the normal groove direction (z-direction), however, the pressure and drag forces are in the same direction, which is also the direction of a very large pressure gradient (see figs. 6 and 7). Therefore, an unbalance of forces exists in this direction. Physically, the $Q = 0$ restriction is not possible. Also, this point can be illustrated from ξ- and η-direction momentum equations, respectively:

$$\frac{\partial^2 u_\epsilon}{\partial \zeta^2} \approx \frac{1}{\mu} \frac{\partial P}{\partial \xi}$$

$$\frac{\partial^2 w_\eta}{\partial \zeta^2} \approx \frac{1}{\mu} \frac{\partial P}{\partial \eta}$$

Notice that there is no velocity "coupling" between the velocity components; that is, u_ϵ and w_η are independent of one another. It is obvious that for zero leakage these velocity components are not independent of one another. Thus, physically as well as mathematically it is not possible under the restrictions of the classical creeping flow analysis to get zero leakage.

Also in the creeping flow analysis the edge effects are assumed negligible. The full meaning of this assumption has not really been clarified; it is only close to physical reality when c is very small and/or b/h_o is very large. For example, the creeping flow analysis is valid for spiral groove thrust bearings where c is on the order of 500 microinches and the aspect ratio is on the order of 1000 ($c/L \ll 1$, see fig. 12). As $b \to h_o$, the edge effect becomes more pronounced as the convective force becomes more and more important. To date only reference 30 has explicitly stated this restriction.

To resolve the paradox of having the drag and pressure forces unbalanced in the z-direction, a convective inertia force is in equilibrium with the pressure and drag forces (a nonlinear effect). The step is causing a convective change that results in generation of an axial pressure gradient. The role of the step is now described.

If a concentric rotor is rotating about a stationary smooth sleeve, no axial pressure gradient is generated. This is the classic axisymmetric Couette flow (see ref. 33). Furthermore, if an axial pressure gradient is imposed (e.g., by having the rotor translate in the axial direction) an "uncoupled" helical flow will result. Subsequently, of course, there will be net flow out.

In the helical groove seal (viscoseal), the step or edge h_o is the pressure generation mechanism. Without the step, that is, the limiting case when $h_o \to 0$ (rotor and

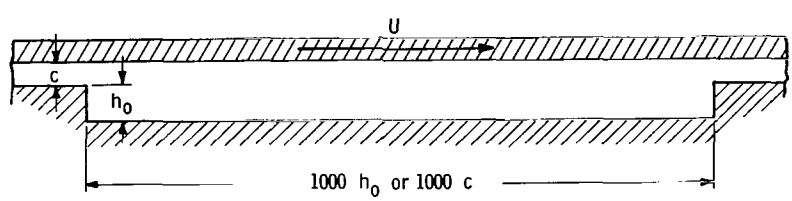

Figure 12. - Example where the creeping flow mathematical model can be considered a valid physical model. Modified Reynolds number (Re^*) much less than 1 since clearance c is much less than characteristic length L.

housing smooth), there is no axial pressure gradient generated. Eccentricity will generate a radial pressure gradient. Therefore, the effect of the groove wall is a convective acceleration or inertia effect (nonlinear effect). To neglect the convective force terms means that the primary axial pressure generating mechanism is neglected.

The creeping flow solution equations are linear and pressure is a potential function. The creeping motion or slow viscous flow momentum equation in vector notation is

$$\nabla P = \mu \nabla^2 \vec{V}$$

The incompressible continuity equation says

$$\nabla \cdot \vec{V} = 0$$

Taking the divergence of both sides of the equation yields

$$\nabla \cdot \nabla P = \mu \nabla^2 (\nabla \cdot \vec{V}) = 0$$

or

$$\nabla^2 P = 0$$

which is Laplace's equation, since pressure is a scalar quantity. Consequently, the multitude of mathematical analog methods of solving linear equations and specifically Laplace's equation can be used. Thus, solutions for end effect can readily be found (refs. 1 and 30).

Muijderman (ref. 1) used conformal mapping to analyze the spiral grooved bearing. Again, this technique can be readily applied because pressure is a potential function.

REFERENCES

1. Muijderman, E. A.: Spiral Groove Bearings. Philips Res. Rept. Suppl. 1964, no. 2.: See also Scientific Lubr., vol. 17, no. 1, Jan. 1965, pp. 12-17.

2. Rowell, H. S.; and Finlayson, D.: Screw Viscosity Pumps. Engineering, vol. 114, Nov. 1922, pp. 606-607.

3. Boon, E. F.; and Tal, S. E.: Hydrodynamic Seal for Rotating Shafts. DEG. Inf. Ser. 13, United Kingdom Atomic Energy Authority, 1961.

4. King, Alan E.: Screw Type Shaft Seals for Potassium Lubricated Generators. IEEE Trans. on Aerospace, vol. AS-3, Supplement, June 1965, pp. 471-479.

5. Ludwig, Lawrence P.; Strom, Thomas N.; and Allen, Gordon P.: Gas Ingestion and Sealing Capacity of Helical Groove Fluid Film Seal (Viscoseal) Using Sodium and Water as Sealed Fluids. NASA TN D-3348, 1966.

6. Ludwig, Lawrence P.; Strom, Thomas N.; and Allen, Gordon P.: Experimental Study of End Effect and Pressure Patterns in Helical Groove Fluid Film Seal (Viscoseal). NASA TN D-3096, 1965.

7. Vohr, J. H.; and Chow, C. Y.: Characteristics of Herringbone-Grooved Gas-Lubricated Journal Bearings. J. Basic Eng., vol. 87, no. 3, Sept. 1965, pp. 568-578.

8. Billet, A. B.: Hydraulic Sealing in Space Environments. Proceedings of the Second International Conference on Fluid Sealing, B. S. Nau, H. S. Stephens, and D. E. Turnbull, eds., British Hydromechanics Research Association, Harlow, Essex, England, 1964, pp. C2-17 - C2-36.

9. Rowell, H. S.; and Finlayson, D.: Screw Viscosity Pumps. Engineering, vol. 126, Aug. 1928, pp. 249-250.

10. Rowell, H. S.; and Finlayson, D.: Screw Viscosity Pumps. Engineering, vol. 126, Sept. 1928, pp. 385-387.

11. Rogowsky, Z.: Mechanical Principles of the Screw Extrusion Machine. Engineering, vol. 162, no. 4213, Oct. 11, 1946, pp. 358-360.

12. Strub, R. A.: Spindle Drag Pump. Machine Design, vol. 25, July 1953, pp. 149-151.

13. Pigott, W. T.: Pressures Developed by Viscous Materials in the Screw Extrusion Machine. ASME Trans., vol. 73, Oct. 1951, pp. 947-955.

14. Anon: Theory of Extrusion. Ind. Eng. Chem., vol. 45, no. 5, May 1953, pp. 969-993.

15. Eccher, Silvio; and Valentinotti, Aldo: Experimental Determination of Velocity Profiles in an Extruder Screw. Ind. Eng. Chem., vol. 50, no. 5, May 1958, pp. 829-836.

16. Griffith, R. M.: Fully Developed Flow in Screw Extruders. Ind. Eng. Chem. Fundamentals, vol. 1, no. 3, Aug. 1962, pp. 180-187.

17. Squires, P. H.: Screw Extrusion - Flow Patterns and Recent Theoretical Developments. SPE Trans., vol. 4, no. 1, Jan. 1964, pp. 7-16.

18. McGrew, J. M.; and McHugh, J. D.: Analysis and Test of the Screw Seal in Laminar and Turbulent Operation. J. Basic Eng., vol. 87, no. 1, Mar. 1965, pp. 153-162.

19. Zotov, V. A.: Research on Helical Groove Seals. Russ. Eng. J., vol. 10, Oct. 1959, pp. 3-7.

20. Asanuma, T.: Studies on the Sealing Action of Viscous Fluids. Paper No. A3 presented at the First International Conference on Fluid Sealing, Cranfield, England. British Hydromechanics Research Association, Harlow, Essex, England, Apr. 1961.

21. Lessley, R. L.; and Hodgson, J. N.: Low-Leakage Dynamic Seal-to-Space. Paper 65-GTP-14, ASME, Feb. 1965.

22. Whipple, R. T. P.: The Inclined Groove Bearing. Rep. AERE-T/R-622 (rev.), Research Group, Atomic Energy Research Establishment, United Kingdom Atomic Energy Authority, 1958.

23. Gruntz, Robert D.; and Rackley, Ray A.: Snap 50/Spur Power Conversion System-Objectives, Current Status and Lunar Applications. Paper No. 650321, SAE, May 1965.

24. Golubiev, A. I.: Studies on Seals for Rotating Shafts of High-Pressure Pumps. Wear, vol. 8, no. 4, July/Aug. 1965, pp. 270-288.

25. Holan, Karel: Sealing in Engineering. Proceedings of the Second International Conference on Fluid Sealings, B. S. Nau, H. S. Stephens, and D. E. Turnbull, eds., British Hydromechanics Research Association, Harlow, Essex, England, 1964, pp. E5-73 - E5-88.

26. Stair, William K.: Analysis of the Visco Seal. Rep. No. ME 65-587-2, University of Tennessee, Jan. 18, 1965.

27. Stair, William K.: Theoretical and Experimental Studies of Visco-Type Shaft Seals. Rep. No. ME 66-587-5, University of Tennessee, Apr. 28, 1966.

28. Lessley, R. L.: Snap-8 Seals-to-Space Development Test Program. vol. 1 - Visco Pump. Rep. No. 2808 (Topical)(NASA CR-54234), Aerojet-General Corp., May 1964.

29. Kettleborough, C. F.: Turbulent and Inertia Flow in Slider Bearings, ASLE Trans., vol. 8, no. 3, July 1965, pp. 286-295.

30. Booy, M. L.: Influence of Oblique Channel Ends on Screw-Pump Performance. J. Basic Eng., vol. 88, no. 1, Mar. 1966, pp. 121-131.

31. Schlichting, Hermann (J. Kestin, Trans.): Boundary Layer Theory. Fourth ed., McGraw-Hill Book, Co., Inc., 1960.

32. Bisson, Edmond E.; and Anderson, William J.: Advanced Bearing Technology. NASA SP-38, 1964.

33. Langlois, W. E.: Slow Viscous Flow. Macmillan Co., 1964, pp. 105-107.

"The aeronautical and space activities of the United States shall be conducted so as to contribute . . . to the expansion of human knowledge of phenomena in the atmosphere and space. The Administration shall provide for the widest practicable and appropriate dissemination of information concerning its activities and the results thereof."

—NATIONAL AERONAUTICS AND SPACE ACT OF 1958

NASA SCIENTIFIC AND TECHNICAL PUBLICATIONS

TECHNICAL REPORTS: Scientific and technical information considered important, complete, and a lasting contribution to existing knowledge.

TECHNICAL NOTES: Information less broad in scope but nevertheless of importance as a contribution to existing knowledge.

TECHNICAL MEMORANDUMS: Information receiving limited distribution because of preliminary data, security classification, or other reasons.

CONTRACTOR REPORTS: Technical information generated in connection with a NASA contract or grant and released under NASA auspices.

TECHNICAL TRANSLATIONS: Information published in a foreign language considered to merit NASA distribution in English.

TECHNICAL REPRINTS: Information derived from NASA activities and initially published in the form of journal articles.

SPECIAL PUBLICATIONS: Information derived from or of value to NASA activities but not necessarily reporting the results of individual NASA-programmed scientific efforts. Publications include conference proceedings, monographs, data compilations, handbooks, sourcebooks, and special bibliographies.

Details on the availability of these publications may be obtained from:

SCIENTIFIC AND TECHNICAL INFORMATION DIVISION

NATIONAL AERONAUTICS AND SPACE ADMINISTRATION

Washington, D.C. 20546